Adsorption of Small Au_n ($n = 1-5$) and Au−Pd Clusters Inside the TS-1 and S-1 Pores

Ajay M. Joshi,† W. Nicholas Delgass,† and Kendall T. Thomson*

School of Chemical Engineering, Purdue University, West Lafayette, Indiana 47907

Received: March 21, 2006; In Final Form: July 6, 2006

We used a hybrid quantum-mechanics/molecular-mechanics (QM/MM) approach to simulate the adsorption of Au_n ($n = 1-5$), AuPd, and Au_2Pd_2 clusters inside the TS-1 and S-1 pores. We studied nondefect and metal-vacancy defect sites in TS-1 and S-1 for a total of four different environments around the T6 crystallographic site. We predict stronger binding of all clusters near Ti sites in Ti-substituted framework compared to adsorption near Si sites—consistent with the experimental finding of a direct correlation between the Ti-loading and the Au-loading on the Au/TS-1 catalysts with high Si/Ti ratio. The cluster binding is also stronger near lattice-metal vacancies compared to fully coordinated, nondefect sites. In all the cases, a trend of binding energy (BE) versus Au cluster size (n) shows a peak at around $n = 3-4$. Our results show that there is enough room for the attack of H_2O_2 on the Ti-defect site even with Au_{1-4} adsorbed—a result that supports the possibility of H_2O_2 spillover from the Au clusters to the adjacent Ti-defect sites. Mulliken charge analysis indicates that in all the cases there is electron density transfer to adsorbed clusters from the zeolite lattice. In the case of both gas-phase and adsorbed Au−Pd clusters, all the Pd atoms were positively charged, and all the Au atoms were negatively charged due to the higher electron-affinity of Au. We also found a correlation between the BE and the charge transfer to the clusters (the higher the charge transfer to the clusters, the higher the BE), and a universal correlation was found for Au_{2-5} when BE and charge transfer were plotted on a per atom basis. A relatively larger charge transfer to the adsorbed clusters was found for the Ti sites versus the Si sites, and for the defect sites versus the nondefect sites. The trends in the BE were corroborated using Gibbs free energy of adsorption (ΔG_{ads}), and the implications of ΔG_{ads} in sintering of Au clusters are also discussed. Our results confirm that electronic factors such as cluster-charging are potentially important support effects for the Au/TS-1 catalyst.

1. Introduction

Au has long been regarded as a poor catalyst due to its noble nature. Hammer and Nørskov[1] have provided a theoretical explanation of why the smooth Au surface is not reactive toward H_2 dissociation. However, in the past few years, Au-based catalysts have captured industrial and scientific attention due to the remarkable catalytic activity of highly dispersed Au particles (≤ 5 nm) deposited on oxide supports.[2,3] Significant advances have been made toward understanding the catalytic activity of nanoscale Au in low-temperature CO oxidation[4−9] and partial oxidation of propylene to propylene oxide.[10−17] Although the Au/TS-1 direct gas-phase propylene epoxidation catalyst has shown a remarkable stability while still maintaining a high selectivity,[18] a substantial improvement in the catalytic activity is needed to qualify for commercialization. A thorough understanding of the nature and location of the active site(s) and catalyst chemistry can provide the rationale to guide that improvement.

Because the TS-1 pore size is approximately 5.5 Å, it is important to note that a major fraction of the Ti sites is actually inside the TS-1 pores. Also, small clusters composed of a few Au atoms may diffuse inside the TS-1 pores and reside near the potentially active Ti sites. In light of these possibilities, it is important to understand whether the external Au/Ti sites or internal Au/Ti sites or both are active toward propylene epoxidation. The TEM observations of the nanometer-sized Au clusters on the active TiO_2 and TS-1 based catalysts do not preclude the existence of internal Au/Ti sites of equivalent or higher activity. Interestingly, recent experiments by Yap et al.[18] have provided an indirect evidence for the potential activity of internal Au/Ti sites in TS-1 for direct gas-phase propylene epoxidation using H_2 and O_2. More direct evidence would be the experimental proof of chemical reactions occurring on the small Au clusters residing inside the TS-1 pores. However, it is very difficult to probe small Au clusters experimentally, particularly clusters consisting of few Au atoms which may reside inside the TS-1 channels.

With these limitations of the experiments to study the catalytic chemistry on small Au clusters, quantum-chemical tools offer a reasonable alternative. Combined computational and experimental strategies are now at the point where theory and experiment can work together and lead to a better understanding of the catalyst function. With growing computer power, quantum-chemical analysis is becoming more and more effective in unraveling catalyst chemistry. As an example, in the case of propylene epoxidation using the TS-1 based catalysts, Wells et al.[19] used density functional theory (DFT) to conclude that at Ti sites adjacent to Si vacancies in TS-1, hydrogen peroxide can partially oxidize propylene to propylene oxide. Recently, they reported a gas-phase catalytic cycle for the formation of hydrogen peroxide from H_2 and O_2 over a neutral Au trimer.[20] This particular study could be regarded as a first step toward understanding the reactivity of small Au clusters in propylene oxidation.

* Corresponding author. E-mail: thomsonk@ecn.purdue.edu. Phone: (765) 496-6706. Fax: (765) 494-0805.
† E-mail: A.M.J., amjoshi@ecn.purdue.edu; W.N.D., delgass@ecn.purdue.edu.

10.1021/jp061754o CCC: $33.50
Published on Web 07/29/2006

The size- and support-dependency of activity of Au based catalysts is well documented.[4] One of the reasons for the special catalytic properties of nanoscale Au catalysts could be a high step density on the small Au particles[21] and the support-dependency could be attributed to the cluster−support interactions,[22] which may lead to the charging of the Au clusters, hence altering their reactivity.[23] Therefore, quantum-chemical analysis should not only consider a wide range of Au cluster sizes but also address the modeling of the Au clusters situated in/on the support.

In this paper, we investigate the interaction of small Au_n ($n = 1-5$) clusters with the interior pore walls of the TS-1 lattice. The Au clusters in this size range may have relatively easy access to the TS-1 interior through the TS-1 pores (∼5.5 Å). Recently, Landon et al. reported a significantly higher liquid-phase H_2O_2 production rate at 2 °C from H_2 and O_2 for Pd−Au catalysts supported on Al_2O_3 than that for Au/Al_2O_3 and Pd/Al_2O_3 catalysts employed under identical conditions.[24] Therefore, it will be interesting to compare the direct gas-phase propylene epoxidation activity of Au−Pd catalysts supported on the TS-1 with that of Au/TS-1 catalysts. As a first step in establishing such a comparison, we also studied the adsorption of the AuPd and Au_2Pd_2 clusters inside the TS-1 pores.

We focused on the T6 crystallographic site of the TS-1 lattice—a representative of the sites at the intersection of the straight channel and the sinusoidal channel—that may have significant contribution to the catalyst activity due to its relatively easy accessibility. Also, the T6 site is one of the possible candidates for the Ti substitution, as demonstrated using powder neutron diffraction.[25] This study established that the distribution of the Ti atoms among the 12 different T sites of the orthorhombic TS-1 lattice is nonuniform and the T6, T7, T11, and to some extent T10 sites are the preferred locations for the Ti substitution.[25] Because the Ti-loading of the TS-1 catalyst is typically 1−2.5 wt %, only 1−3 Ti-sites can be found per unit cell of TS-1. Therefore, any species entering the TS-1 lattice would interact not only with the Ti sites but also with the purely siliceous sites (S-1). Therefore, we investigated the interaction of small Au ensembles with both Ti sites (with a Ti atom located at the T6 crystallographic position) and Si sites (no Ti atom in the cluster model but maintaining the orthorhombic structure). Although we are calling our purely siliceous cluster model S-1, the as-synthesized orthorhombic S-1 framework converts to a monoclinic form upon calcination (however, this is not the case for TS-1). For both the Ti- and Si-site models, we considered two different types of sites: a nondefect site and a defect site. The details of these sites are discussed in the next section. In each case, we considered many different starting positions for the Au clusters and discovered the most favorable (lowest energy or ground state) configuration for the Au clusters anchored inside the TS-1 lattice.

In their DFT study, Wells et al.[19] reported a mechanism for propylene oxidation to propylene oxide using H_2O_2 as the oxidizing agent, with a T6 Ti-defect site as the active site. However, their focus was the liquid-phase epoxidation process (H_2O_2/TS-1) and hence they did not include Au clusters in their calculations. In the context of direct propylene epoxidation using H_2 and O_2 over an Au/TS-1 catalyst, it is important to investigate whether there is enough space for H_2O_2 and/or propylene to react on the T6 Ti-defect site when Au clusters are in its vicinity. Wells et al.[20] also reported a H_2O_2 formation pathway from H_2 and O_2 on the gas-phase Au_3, and the current authors have recently extended this work to H_2O_2 formation on larger clusters (Au_4^+, Au_5, and Au_5^-)[26] and propylene epoxidation on Au_3.[27] Anchoring of the Au clusters at nondefect and defect Ti-sites would also throw light on the possibility of spillover of H_2O_2 formed on anchored Au clusters to the neighboring active Ti sites inside the TS-1 pores. Finally, we are also interested in the ability of Au−Pd alloy clusters supported in/on the TS-1 to produce H_2O_2 from H_2 and O_2.

A conventional way to model the active sites of zeolites involves performing pure quantum mechanical (QM) calculations on a cluster model consisting of a finite number of T sites. Due to computer-time constraints such cluster models are usually restricted to a small number of T sites (typically 5−8), which fail to replicate the effect of stearic constraints imposed by the zeolite pores and also ignore the long-range interactions (due to dispersion forces) with the rest of the framework. A better model should make up for these inadequacies in the conventional modeling schemes. A popular scheme is to use a hybrid methodology with both quantum- and molecular-mechanics calculations.[28−33] Such a QM/MM scheme can involve a large number of T sites (large cluster) to account for the stearic effects. However, quantum-mechanical (QM) calculations are performed only on a subset of T sites (a relatively small cluster) to simulate the local reactivity accurately. The rest of the framework is represented by molecular mechanics (MM), which typically involves use of force fields.[34,35] Several studies in the literature have highlighted the advantages of such hybrid QM/MM calculations in simulating the reaction environments of zeolites and other materials.[33,36−39]

We carried out an embedded-cluster modeling (QM/MM) of the TS-1 lattice for our analysis of the Au cluster anchoring using the ONIOM[40] scheme available in the Gaussian 03 suite of programs.[41] We used electronic density-functional theory (DFT) to model the quantum mechanical (QM) part and the universal force field (UFF)[35] to model the molecular mechanical (MM) part of our calculations. The details of our methodology are discussed in the following section.

2. Computational Methods and Cluster Models

We used a finite cluster approximation to model the T6 site in the MFI framework of TS-1. It is necessary to have a sufficiently large zeolite cluster to model the interactions of Au clusters as large as Au_5 (and Au−Pd clusters) with the TS-1 pore walls. It is impractical to perform quantum mechanical (QM) calculations on a cluster as large as a unit cell of the MFI framework. It is well established in the literature that the hybrid QM/MM calculations offer a very good alternative to model the reactive environment around the T sites in the zeolites.[30,33,37,39,42] Moreover, DFT cannot properly account for the dispersion interactions that are likely to affect the adsorption/reaction energetics. These interactions can be better accounted for by augmenting the DFT (QM) calculations with force field-based MM calculations. In fact, Sauer and co-workers have demonstrated the use of their ion-pair-shell-model type of force field to perform QM/MM calculations on the Ti−silicalite catalysts.[43]

In Figure 1, we show a picture of our embedded-cluster model of the T6 site in TS-1. The cluster consists of two regions: (1) the inner core region and (2) the outer region. The inner core region consists of the T6 site and 10 nearest-neighbor T sites around it (total 11 T sites). The outer region consists of 108 T sites located around the core region containing 11 T sites. Therefore, our embedded-cluster model consists of a total of 119 T sites. Kasuriya et al.[30] also used a two layer QM/MM scheme to study the adsorption of hydrocarbons over the fujasite zeolites and reported that the energetics of the system converged at a cluster size of 84 T. Our embedded-cluster model with 119 T sites is sufficiently large to achieve a convergence with respect

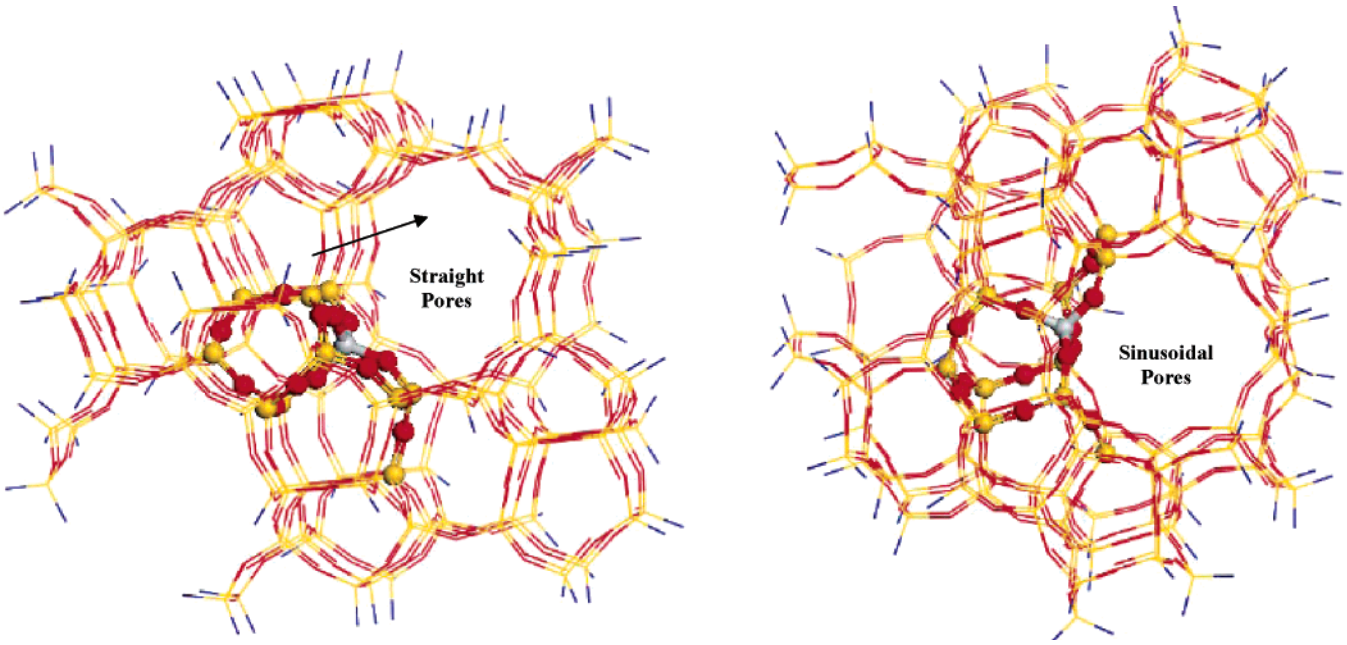

Figure 1. Embedded-cluster model of the TS-1 lattice. The QM region is made up of 11 T sites and is represented by the ball-and-stick display format. The MM region is made up of 108 T sites and is represented by the wire-mesh format. The MM region has terminal H atoms at the periphery. Ti atom: gray ball. Si atoms: yellow balls and wires. O atoms: red balls and wires. H atoms: blue wires.

to the long-range interactions due to van der Waals forces. It should also be noted that this cluster represents the straight and the sinusoidal pores of the TS-1 completely. At the *outer* periphery of the embedded-cluster model, Si−H terminations were used to satisfy the valences of the peripheral Si atoms. These peripheral Si−H terminations were fixed at a Si−H bond length of 1.47 Å, which was decided on the basis of the level of theory used for the respective layer.

Our embedded-cluster calculations were performed using the two layer ONIOM[40] scheme available in the Gaussian 03 suite of programs.[41] The calculation of the ONIOM energy involves three subcalculations:[40] (1) higher level (QM) calculation on the inner or core region of the cluster, (2) lower level (MM) calculation on the inner or core region of the cluster, and (3) lower level (MM) calculation on the complete embedded-cluster (inner + outer region together). The ONIOM extrapolation formula is as follows: $E(\text{ONIOM}) = E(1) - E(2) + E(3)$. Again, Si−H terminations were used while the calculation was performed on the inner or core region. The details regarding the positions of these H terminations can be found in the paper by Dapprich et al.[40] In a recent study of the reactivity of Ti sites in TS-1 for propylene epoxidation, Wells et al.[19] from our group employed the BPW91/LANL2DZ method. However, they considered only full QM calculations with 8 T sites in their cluster model. The choice of 11 T sites (in the QM region) for current work was dictated by the full QM calculations performed with 5, 11, and 17 T sites to model the anchoring of Au_{1-5} clusters. We found that the cluster adsorption energies in a full QM cluster model with 11 and 17 T sites differ only by 1−2 kcal/mol, and hence believe that the adsorption energies would converge with only 11 T sites in the QM part of the QM/MM embedded-cluster calculations. Also, there is a significant computer-time savings in calculations with 11 QM T sites over those with 17 QM T sites. We have already stated that our embedded-cluster (QM + MM) model with 119 T sites is sufficiently large to achieve convergence with respect to the long-range interactions. We performed test QM/MM calculations of Au_3 adsorption on the Ti-nondefect site using 11 T sites and 17 T sites in the QM region. We found that the BE only increased by 1.2 kcal/mol when 17 T sites were included in the QM region, indicating that for all practical purposes our QM/MM results are converged with 11 T sites in the QM region.

We continued using the BPW91 density-functional,[44−46] LANL2DZ pseudo-potential,[47,48] and the corresponding double-ζ basis set to perform the higher level (QM) calculations in the ONIOM scheme. To test the accuracy of the BPW91/LANL2DZ method, we carefully investigated the effect of using a more complete basis set augmented with diffuse and polarization functions. We found that the binding energies are reduced by 2.2−5.1 kcal/mol (for Au_3), but that the main findings reported in this paper are essentially unchanged even when a better basis set is employed. The details of this analysis are available in the Supporting Information to this paper. Molecular mechanics and the universal force field (UFF)[35] were employed to perform the lower level calculations. The UFF atom types for Ti, Si, O, H, Pd, and Au were identified to be Ti3+4, Si3, O_3_z, H_, Pd4+2, and Au4+3, respectively.[35] In this nomenclature the number following the chemical symbol represents the hybridization or geometry (3 for tetrahedral and 4 for square planar) which is followed by the formal oxidation state, e.g., +4 formal oxidation state for Ti atom; O_3_z is an oxygen suited for framework oxygens of a zeolite lattice. All the calculations were performed using the Gaussian 03 suite of programs.[41] The Mulliken charge analysis was carried out on all optimized geometries using the in-built tools in the Gaussian 03 software.[41]

There are two main reasons to use such hybrid calculations: (1) to simulate the straight and sinusoidal pores of TS-1, which is necessary to account for the stearic effects, and (2) to account for the long-range interactions due to dispersion forces. To achieve this objective, we fixed all the atoms in the outer layer to their respective crystallographic positions. Such a methodology also helps in reducing the errors due to any inaccuracies in the force field parameters. Following the work by Sierka and Sauer,[29] who used the disiloxane and octahydridosilasesquioxane molecules to test the accuracy of their ion-pair-shell-potentials, we performed test calculations on the disiloxane ($H_3Si-O-SiH_3$) molecule, as the Si−O−Si bond of disiloxane represents the Si−O−Si linkage in zeolites. We found that the UFF

underpredicts the Si−O bond length by 0.05 Å. This means that the geometry relaxation (optimization) of the outer layer of the embedded-cluster may result in an inappropriate geometry for the outer layer of the cluster and may fail to simulate the stearic constraints properly. Therefore, as stated earlier, we fixed all the outer layer atoms to their respective crystallographic positions and simulated the pore structure correctly; such an arrangement would also be able to represent the rigidity of the zeolite cage. To obtain accurate quantitative results, it is necessary to allow a full relaxation of the active site and the local environment around it (neighboring T sites and O atoms); such local interactions/effects are expected to have a major contribution in the adsorption energy. Therefore, we allowed a full geometry optimization (without any constraints) of all 11 T sites and O atoms linked to them in the inner (or core) region of the embedded-cluster. In short, we allowed the relaxation of all the Ti, Si, and O QM atoms in our model.

In QM/MM calculations, the effect of long-range electrostatic interactions can be accounted for either by a mechanical embedding scheme or by an electronic embedding scheme. The absolute energies are very sensitive to the partial charge values, and because the scheme of charge equalization (qeq) and the qeq charges depend on the geometry, they would change during each step of the geometry optimization. Thus, due to the potential negative effect on the robustness of the geometry optimization scheme, the Gaussian 03[41] software package does not account for the qeq charge calculation at each geometry step. Therefore, a very complicated and recursive manual scheme is needed to account for the effects of partial charges.

In a recent QM/MM study of C_6 diene cyclization in HZSM-5 from our group, Joshi and Thomson[37] analyzed the effects of these partial charges and charge equilibration issues. They carried out a careful comparison of the energetics with and without a method to account for the force field based partial charges and charge equilibration. They concluded that with a large enough QM level cluster, partial charges in the MM region cause approximately constant shifts in the energetics. Because that particular study was similar to this work, consisting of a QM level cluster model with 11 T sites, it is reasonable to assume that their conclusions are applicable to our study. Also, we believe that our 11 T site QM level model is large enough to account for all important local electrostatic interactions which would affect the Au cluster adsorption process. Therefore, for the QM/MM results reported in this paper, we have used only those terms of UFF that do not depend on partial charges.

If all the T sites of a zeolite are tetrahedrally connected to each other through T−O−T linkages, then the zeolite framework is without any defects. However, even for a well made TS-1, it is possible to find an unoccupied T site (metal-vacancy defect in the zeolite) that results in the formation of a local silanol nest.[25,49] The simulation results reported by Wells et al.[19] suggest that it is not unlikely to find approximately one Ti/defect pair (a Ti site neighboring a defect, i.e., missing Si at the neighboring site) per unit cell of the TS-1, at 2% Ti substitution level, 8% defect frequency, and random location of Ti substitution and defect occurrences on the Lamberti subset[25] (T6, T7, T11, and T10). In Figure 2, we show the models of nondefect and defect T sites. In the case of the nondefect site, the T site of interest (T6 in this study) is connected to four neighboring T sites through O atoms of the T−O−T linkages, and each of these neighboring sites also has four T−O−T linkages. If one of the neighboring T sites is absent, then the T site of our interest has three T−O−T linkages and one T−OH group attached to it, and is termed a defect site. There are three more (a total of four) T−OH groups formed due to the three other neighbors of the missing T site. So a defect Ti site (hereafter denoted as T6-Ti-defect) has a Ti atom at the T6 site and one neighboring Si of the T6 Ti site is missing. Around the missing Si, a silanol nest is formed, with three Si−OH and one Ti−OH groups. In the case of a defect Si site (hereafter denoted as T6-Si-defect), there are four Si−OH groups in the silanol nest.

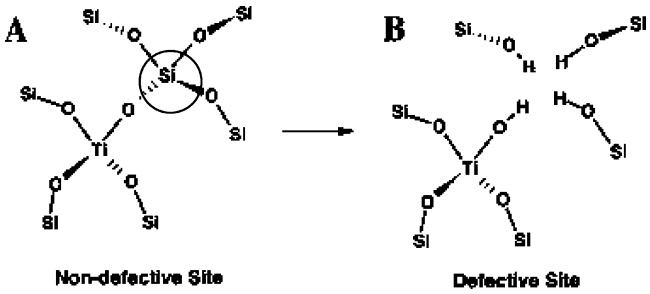

Figure 2. Schematic view of a fully tetrahedrally bonded Ti ion substituted for a Si ion at one of the lattice positions of TS-1 (A) and the same Ti site located near a silicon vacancy terminated with hydroxyl groups forming a silanol nest (B). Reprinted from ref 19.

In our QM/MM calculations, we considered several different starting orientations for the Au_n ($n = 1-5$) and Au−Pd clusters inside the TS-1 pores and allowed a full geometry optimization to obtain the adsorbed configuration. We considered anchoring of the clusters in the straight channel, in the sinusoidal channel, and at the junction of the two channels, with different anchoring configurations (at least 12). We selected the lowest energy adsorbed configuration (ground state) for further analysis and all the results reported in this paper are concerned with only the ground-state adsorbed configuration of each of the Au_n ($n = 1-5$) and Au−Pd clusters. We confirmed the stability of the adsorbed configurations by verifying that all the vibrational frequencies are positive. A cluster entering the TS-1 pores can anchor at any of the following four sites: (1) T6-Ti-nondefect, (2) T6-Si-nondefect, (3) T6-Ti-defect, and (4) T6-Si-defect. Therefore, aforementioned procedure was actually repeated for each of these four sites.

We calculate the binding energy (BE) of a given Au_n cluster as follows: $BE(Au_n) = E(Au_n) + E(\text{T site}) - E(Au_n\text{-T-site})$, where $E(Au_n)$ is the electronic energy of the ground-state configuration of the Au_n cluster in a vacuum, E(T-site) is the ONIOM energy of the TS-1 embedded cluster for the specific type of site, and $E(Au_n\text{-T-site})$ is the ONIOM energy of the ground-state configuration of the Au_n cluster adsorbed on the specific T site type inside the TS-1 pores. Therefore, BE is negative of the (electronic) adsorption energy; i.e., a positive binding energy indicates exothermic adsorption. A similar formula was used to determine the BE of AuPd and Au_2Pd_2 clusters. The dispersion-type interactions between fully occupied d-shells in Au/Pd atoms and lattice atoms of TS-1/S-1 are likely to contribute to the BE of Au/Au−Pd clusters.[50] Our QM/MM-based BE values include contribution from these important interactions. Because a similar embedded cluster (QM region, 11 T sites; total, 119 T sites) was employed to model all four sites, it is likely that the contribution of force fields to the BE of a given Au/Au−Pd cluster adsorbed on these four sites is similar. Therefore, in Table 1 we only report the contribution of force fields (BE_{MM}) for adsorption of Au/Au−Pd clusters on a Ti-defect site and assume that similar contributions are likely for adsorption on the other three sites. We used the following formula to calculate the BE_{MM} for a given Au/Au−Pd cluster: $BE_{MM} = BE - BE_{QM}$. Here, BE is the binding energy of a given Au/Au−Pd cluster calculated using the QM/

TABLE 1: Binding Energies (BE) of Au_n ($n = 1-5$), AuPd, and Au_2Pd_2 Clusters Adsorbed on T6-Ti-Nondefect, T6-Si-Nondefect, T6-Ti-Defect, and T6-Si-Defect Sites Inside the TS-1 Pores[a]

	BE (kcal/mol) of Au and Au−Pd clusters on different sites			
cluster	Ti-nondefect	Si-nondefect	Ti-defect	Si-defect
Au_1	4.80	2.13	9.18 (5.22)	4.17
Au_2	18.32	15.93	24.89 (6.95)	18.72
Au_3	17.56	15.57	28.17 (8.29)	22.31
Au_4	18.91	17.43	30.19 (12.01)	21.17
Au_5	7.84	7.28	19.43 (6.43)	17.28
AuPd	17.09	16.05	23.27 (5.03)	21.16
Au_2Pd_2	16.69	14.47	24.00 (8.04)	17.56

[a] All the data (except the values in brackets) in this table are based on the ground-state configurations of the adsorbed clusters obtained using QM/MM calculations. The values in parentheses represent the contribution of the force fields to the binding energy (BE_{MM}).

MM calculations and BE_{QM} is the binding energy of the same Au/Au−Pd cluster calculated by performing pure QM calculation (geometry optimization) on Si−H terminated 11 T site cluster model of Ti-defect site in TS-1.

We also report a full thermochemical analysis of our QM/MM calculations and verify the trends in the BE using Gibbs free energy of adsorption (ΔG_{ads}) calculated at 298.15 K and 1 atm (Table 7). We note that a negative value of ΔG_{ads} indicates spontaneous (favorable) adsorption.

3. Results

We now discuss our results on adsorption of Au_{1-5}, AuPd, and Au_2Pd_2 clusters on the T6-Ti-nondefect, T6-Si-nondefect, T6-Ti-defect, and T6-Si-defect sites obtained using the embedded-cluster (QM/MM) calculations. A first step in this study is to find the ground-state geometries of Au and Au−Pd clusters in the gas phase. We discuss only the important details of the gas-phase cluster geometries in this paper; figures are not included as they are available in several other papers cited later in this section. For adsorbed geometries, because we have seven different clusters and four different types of sites, there are a total of 28 ground-state geometries of adsorbed clusters. For the sake of brevity, we provide figures of clusters adsorbed on the T6-Ti-defect site only (Figures 3−9). The atom no. 409 in Figure 8 and atoms 410 and 411 in Figure 9 are Pd atoms. The BEs of all seven clusters are reported in Table 1.

It is well-known that in the case of supported Au clusters, catalytic activity is sensitive to Au−support interactions.[4,23] Therefore, we report the Mulliken charge analysis for the adsorbed configurations and for four different types of sites without any adsorbed cluster for comparison (see Table 2). We want to point out that the "net charge on the cluster" reported in the Tables 3−6 and in the text refers to the total Mulliken charge on the adsorbed Au or Au−Pd alloy clusters.

3.1. Au_1 and Au_2. A single atom of Au adsorbs rather weakly on all four types of sites. Although the BEs are positive (exothermic adsorption) in all four cases, the Gibbs free energy of adsorption (ΔG_{ads}) of single Au atom on these sites is positive or only slightly negative due to entropy-loss upon adsorption. It should be noted that in all four cases, the Au-T6 (Au−Ti or Au−Si) distance is more than 3 Å, indicating a lack of close interaction upon adsorption. Pacchioni and co-workers[51,52] also found that the interaction between the Au/Pd atoms and the nondefect silica surface is weak and presence of defects such as ≡S−O• or ≡S−O$^-$ is responsible for trapping of adsorbed atoms due to much stronger interaction. Moreover, they found that although the Au (and Pd) atom interacts weakly with the SiO_2/Mo(112) film, it forms a direct covalent bond with the Ti centers in a Ti-doped SiO_2/Mo(112) film.[53] However, we found a relatively smaller difference in the strength of interaction of Au with S-1 and TS-1. This is probably due to the difference in the nature of supports investigated by Pacchioni and co-workers and us. Nevertheless, we also found somewhat stronger adsorption of Au atoms on Ti sites than on Si sites.

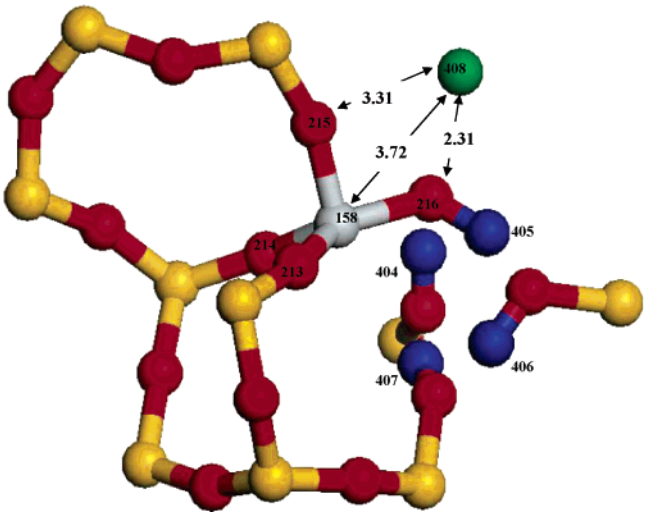

Figure 3. Au_1 adsorbed on the T6-Ti-defect site of the TS-1 lattice. All the molecular-mechanics atoms and some atoms in the quantum-mechanics region are removed for clarity. The numbers near arrows represent the atomic distances in Å. The atom labels are consistent with the column named "no." in Tables 2−6. Ti atom: gray ball. Si atoms: yellow balls. O atoms: red balls. H atoms: blue balls. Au atom: green ball.

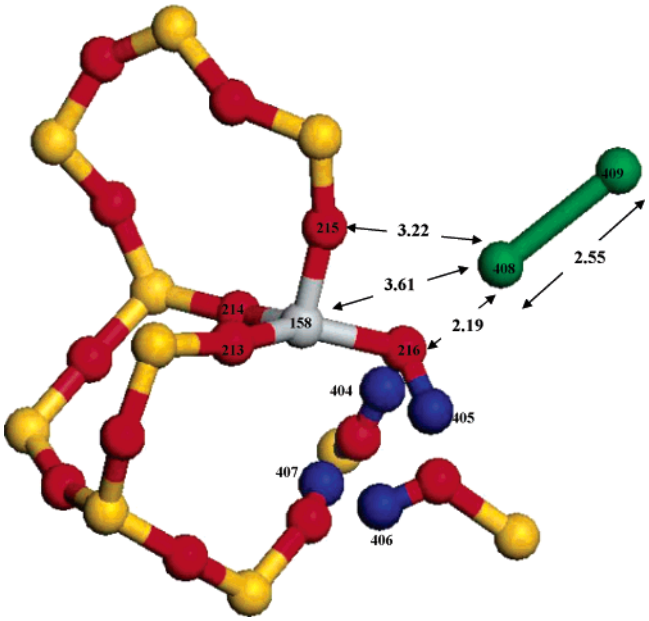

Figure 4. Au_2 adsorbed on the T6-Ti-defect site of the TS-1 lattice. All the molecular-mechanics atoms and some atoms in the quantum-mechanics region are removed for clarity. The numbers near arrows represent the atomic distances in Å. The atom labels are consistent with the column named "no." in Tables 2−6. Ti atom: gray ball. Si atoms: yellow balls. O atoms: red balls. H atoms: blue balls. Au atoms: green balls.

Compared to Au_1, Au_2 adsorption is much stronger, but the Au−Au bond length remains close to the gas-phase value of 2.54 Å. Of particular interest is a strong binding of Au_2 on the Ti-defect site, with a binding energy of 24.89 kcal/mol, significantly higher than 9.18 kcal/mol for Au_1. Correspond-

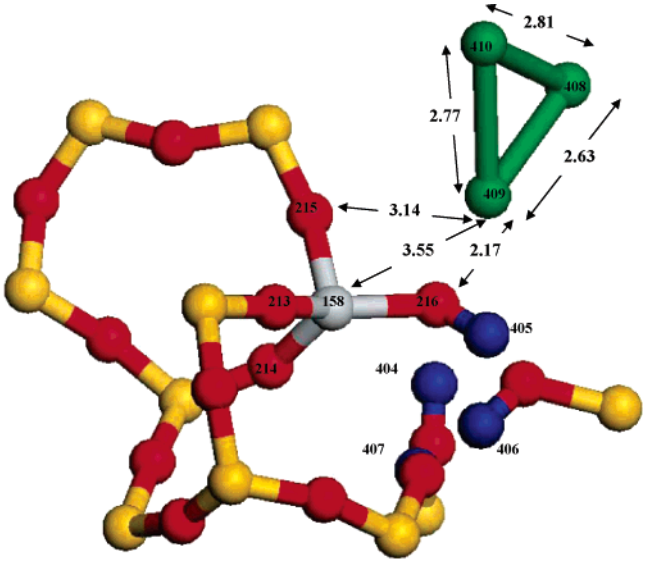

Figure 5. Au_3 adsorbed on the T6-Ti-defect site of the TS-1 lattice. All the molecular-mechanics atoms and some atoms in the quantum-mechanics region are removed for clarity. The numbers near arrows represent the atomic distances in Å. The atom labels are consistent with the column named "no." in Tables 2−6. Ti atom: gray ball. Si atoms: yellow balls. O atoms: red balls. H atoms: blue balls. Au atoms: green balls.

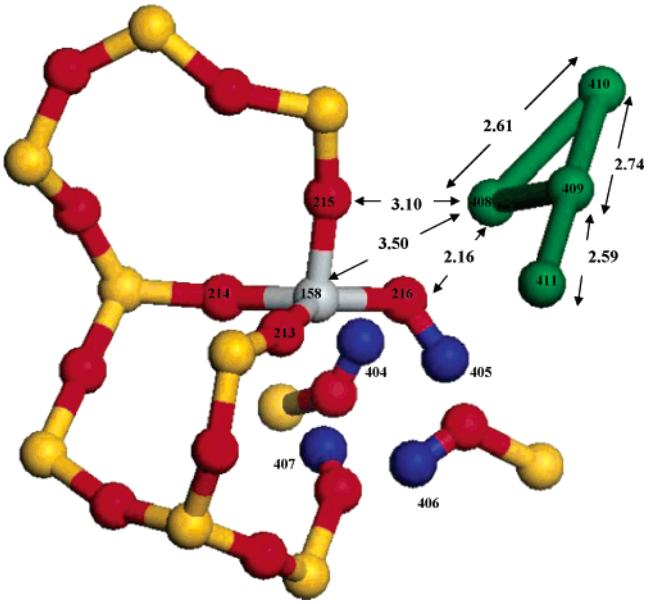

Figure 6. Au_4 adsorbed on the T6-Ti-defect site of the TS-1 lattice. All the molecular-mechanics atoms and some atoms in the quantum-mechanics region are removed for clarity. The numbers near arrows represent the atomic distances in Å. The atom labels are consistent with the column named "no." in Tables 2−6. Ti atom: gray ball. Si atoms: yellow balls. O atoms: red balls. H atoms: blue balls. Au atoms: green balls.

ingly, the closest Au−O distance decreases from 2.31 (Au_1) to 2.19 Å (Au_2). In all the cases, Au_2 adsorbs at the intersection of straight and sinusoidal channels and ΔG_{ads} is significantly negative, indicating thermodynamically favorable adsorption.

Au_1 adsorbed on all four sites showed a slight negative charge on it; hence the Au−support interaction results in charge (electron) transfer to Au anchored on the TS-1 support. Similar results were found for Au_2. However, in the case of Au_2, the adsorbed Au_2 cluster exhibited significant charge polarization. The Au atom proximal to the lattice T6 site had a positive charge

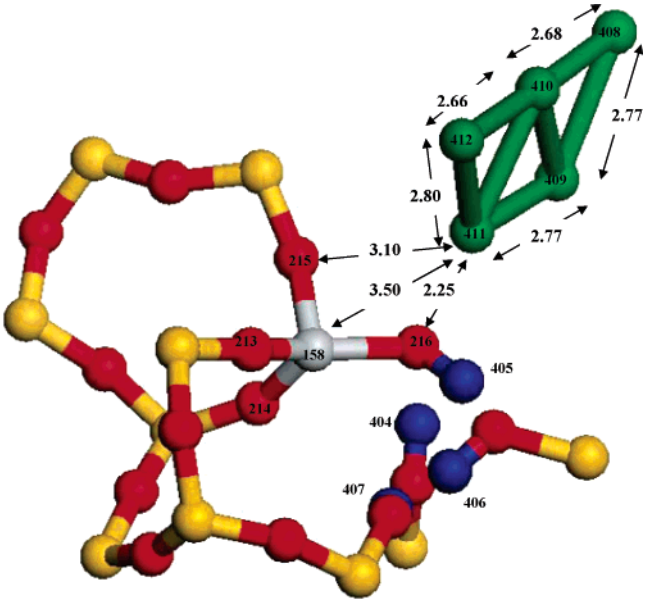

Figure 7. Au_5 adsorbed on the T6-Ti-defect site of the TS-1 lattice. All the molecular-mechanics atoms and some atoms in the quantum-mechanics region are removed for clarity. The numbers near arrows represent the atomic distances in Å. The atom labels are consistent with the column named "no." in Tables 2−6. Ti atom: gray ball. Si atoms: yellow balls. O atoms: red balls. H atoms: blue balls. Au atoms: green balls.

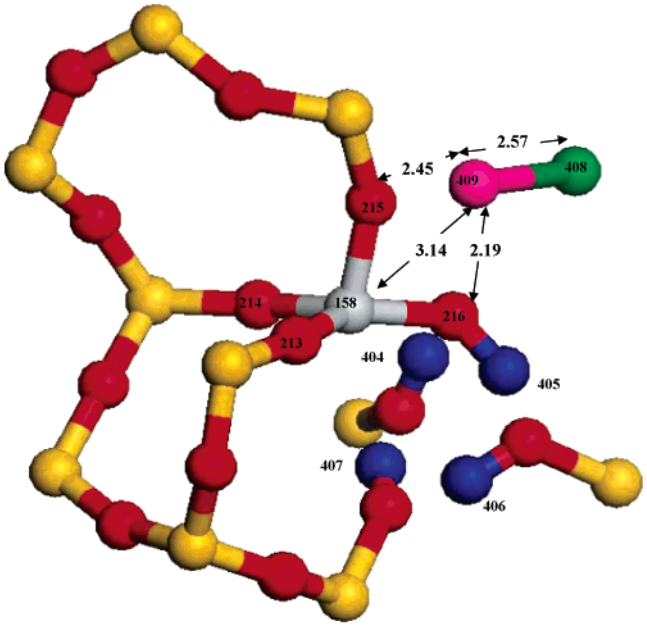

Figure 8. AuPd adsorbed on the T6-Ti-defect site of the TS-1 lattice. All the molecular-mechanics atoms and some atoms in the quantum-mechanics region are removed for clarity. The numbers near arrows represent the atomic distances in Å. The atom labels are consistent with the column named "no." in Tables 2−6. Ti atom: gray ball. Si atoms: yellow balls. O atoms: red balls. H atoms: blue balls. Au atoms: green balls. Pd atom: pink ball.

(due to its proximity to electronegative lattice O atoms) and the distal Au atom had a significant negative charge. However, the overall or net charge on Au_2 was still negative. It should also be noted that in all four cases the net negative charge on Au_2 was greater than that on Au_1. We note that a recent DFT study of adsorption of Au_1 and Au_2 on TiO_2(110) also shows negative charging of adsorbed Au-clusters.[54]

A comparison of charges on the zeolite framework with and without adsorbed Au_1 shows that for nondefect sites, T6-Ti (or

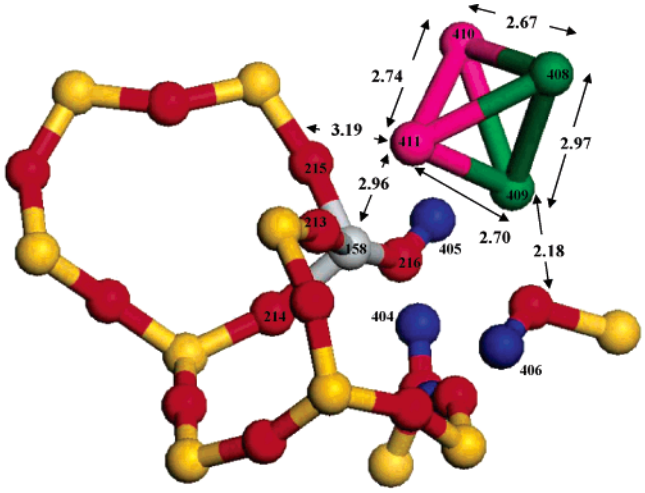

Figure 9. Au_2Pd_2 adsorbed on the T6-Ti-defect site of the TS-1 lattice. All the molecular-mechanics atoms and some atoms in quantum-mechanics region are removed for clarity. The numbers near arrows represent the atomic distances in Å. The atom labels are consistent with the column named "no." in Tables 2−6. Ti atom: gray ball. Si atoms: yellow balls. O atoms: red balls. H atoms: blue balls. Au atoms: green balls. Pd atom: pink ball.

TABLE 2: Mulliken Charge Analysis of the Four Different Kinds of Environments/Sites Studied in This Paper[a]

T6-Ti-nondefect			T6-Si-nondefect		
no.	atom	charge	no.	atom	charge
158	T6 Ti	+1.35	158	T6 Si	+1.85
214	O^t	−0.79	214	O^t	−0.98
215	O^t	−0.82	215	O^t	−0.95
216	O^t	−0.74	216	O^t	−0.89
217	O^t	−0.76	217	O^t	−0.92
221	O	−0.93	221	O	−0.95
T6-Ti-defect			**T6-Si-defect**		
no.	atom	charge	no.	atom	charge
158	T6 Ti	+1.42	158	T6 Si	+1.83
213	O^s	−0.85	213	O^s	−0.98
214	O^s	−0.82	214	O^s	−0.96
215	O^s	−0.77	215	O^s	−0.94
216	O^s	−0.76	216	O^s	−0.95
404	H^s	+0.48	404	H^s	+0.52
405	H^s	+0.48	405	H^s	+0.52
406	H^s	+0.50	406	H^s	+0.50
407	H^s	+0.51	407	H^s	+0.50

[a] The data for O atoms directly connected to the T6 site is marked by a superscript "t". The O and H atoms of the silanol nest are marked with a superscript "s". The unmarked atoms are other lattice atoms near the T6 site. The column "no." reports the serial numbers of the atoms.

Si) and the O atom closest to the adsorbed Au atom contributed to the electron transfer. In the case of Au_1 anchored on defect sites, the T6-Ti (or Si) atom and H atoms of the Ti/Si−OH groups lost some electron-density to Au_1. In the case of Au_2 anchored on both nondefect and defect sites, T6-Ti (or Si) atoms lost significant electron-density to the adsorbed Au_2. It should be noted that in most of the cases, the negative charges on lattice O atoms were unchanged upon adsorption. However, noting that the Au atoms were closer to the lattice O atoms than to the T6 Ti or Si site, it is reasonable to postulate that Au atoms extracted electron density from the negatively charged lattice O atoms, which in turn extracted it from Ti or Si sites. Therefore, lattice O atoms act as agents to carry out a rather long-distance electron transfer from Ti or Si sites to the adsorbed Au clusters.

The observed (net) negative charge on adsorbed Au clusters is reasonable considering that the electron affinity of all the

TABLE 3: Mulliken Charge Analysis of the Au_{1-4} Clusters Adsorbed on the T6-Ti-Nondefect and T6-Si-Nondefect Sites[a]

T6-Ti-nondefect			T6-Si-nondefect		
no.	atom	charge	no.	atom	charge
	Au_1	**−0.16**		**Au_1**	**−0.10**
158	T6 Ti	+1.42	158	T6 Si	+1.87
216	O^t	−0.74	217	O^t	−0.92
217	O^t	−0.73	221	O	−0.94
221	O	−0.92			
	Au_2	**−0.27**		**Au_2**	**−0.15**
158	T6 Ti	+1.58	158	T6 Si	+1.90
214	O^t	−0.78	214	O^t	−0.97
215	O^t	−0.81	215	O^t	−0.94
216	O^t	−0.86	216	O^t	−0.97
217	O^t	−0.74	217	O^t	−0.93
	Au_3	**−0.23**		**Au_3**	**−0.18**
158	T6 Ti	+1.44	158	T6 Si	+1.87
215	O^t	−0.81	215	O^t	−0.96
216	O^t	−0.71	216	O^t	−0.89
217	O^t	−0.75	217	O^t	−0.92
221	O	−0.96	221	O	−0.97
	Au_4	**−0.28**		**Au_4**	**−0.18**
158	T6 Ti	+1.59	158	T6 Si	+1.90
214	O^t	−0.79	214	O^t	−0.97
215	O^t	−0.81	215	O^t	−0.94
216	O^t	−0.85	216	O^t	−0.99
217	O^t	−0.75	217	O^t	−0.92

[a] The charge reported for the Au_n cluster corresponds to the "net charge" on the whole cluster. For the sake of brevity only important lattice atoms are included.

TABLE 4: Mulliken Charge Analysis of the Au_5, AuPd, and Au_2Pd_2 Clusters Adsorbed on the T6-Ti-Nondefect and T6-Si-Nondefect Sites[a]

T6-Ti-nondefect			T6-Si-nondefect		
no.	atom	charge	no.	atom	charge
	Au_5	**−0.16**		**Au_5**	**−0.13**
158	T6 Ti	+1.38	158	T6 Si	+1.84
214	O^t	−0.79	214	O^t	−0.98
215	O^t	−0.82	215	O^t	−0.95
216	O^t	−0.73	216	O^t	−0.89
217	O^t	−0.77	217	O^t	−0.93
	AuPd	**−0.14**		**AuPd**	**−0.09**
	Au	−0.58		Au	−0.53
	Pd	+0.44		Pd	+0.44
158	T6 Ti	+1.48	158	T6 Si	+1.89
214	O^t	−0.78	214	O^t	−0.97
216	O^t	−0.86	216	O^t	−0.98
217	O^t	−0.74	217	O^t	−0.93
	Au_2Pd_2	**−0.13**		**Au_2Pd_2**	**−0.06**
	Au_2	−0.71		Au_2	−0.77
	Pd_2	+0.58		Pd_2	+0.71
158	T6 Ti	+1.55	158	T6 Si	+1.89
214	O^t	−0.79	214	O^t	−0.97
215	O^t	−0.82	215	O^t	−0.94
216	O^t	−0.86	216	O^t	−0.98
217	O^t	−0.75	217	O^t	−0.93

[a] The charge reported for the cluster corresponds to the "net charge" on the whole cluster. The "effective charge" on the Au and Pd portions is also reported for the alloy clusters. For the sake of brevity only important lattice atoms are included.

Au clusters[55] in this study has been shown to be greater than that of the O atom.[56] Hence, we expect the (partial) negatively charged bridging oxygen to donate charge to the more electronegative Au cluster. In the case of Au_2, the transferred charge is redistributed, or polarized, on the Au cluster, to minimize Coulomb repulsion with the negatively charged lattice O atoms, which is why we see a partial positive charge on the Au atom proximal to the lattice oxygen (net or total charge on Au_2 is

TABLE 5: Mulliken Charge Analysis of the Au_{1-4} Clusters Adsorbed on the T6-Ti-Defect and T6-Si-Defect Sites[a]

T6-Ti-defect			T6-Si-defect		
no.	atom	charge	no.	atom	charge
	Au_1	**−0.29**		**Au_1**	**−0.18**
158	T6 Ti	+1.59	158	T6 Si	+1.86
213	O^s	−0.82	214	O^s	−0.95
215	O^s	−0.76	215	O^s	−0.96
216	O^s	−0.83	216	O^s	−0.94
	Au_2	**−0.36**		**Au_2**	**−0.23**
158	T6 Ti	+1.63	158	T6 Si	+1.87
213	O^s	−0.84	213	O^s	−0.98
214	O^s	−0.81	214	O^s	−0.95
215	O^s	−0.75	215	O^s	−0.97
216	O^s	−0.84	216	O^s	−0.96
	Au_3	**−0.41**		**Au_3**	**−0.24**
158	T6 Ti	+1.66	158	T6 Si	+1.86
213	O^s	−0.83	213	O^s	−0.98
214	O^s	−0.81	214	O^s	−0.95
215	O^s	−0.76	215	O^s	−0.97
216	O^s	−0.86	216	O^s	−0.97
	Au_4	**−0.43**		**Au_4**	**−0.25**
158	T6 Ti	+1.67	158	T6 Si	+1.87
213	O^s	−0.83	213	O^s	−0.98
214	O^s	−0.81	214	O^s	−0.95
215	O^s	−0.76	215	O^s	−0.97
216	O^s	−0.85	216	O^s	−0.96

[a] The charge reported for the Au_n cluster corresponds to the "net charge" on the whole cluster. For the sake of brevity only important lattice atoms are included.

TABLE 6: Mulliken Charge Analysis of the Au_5, AuPd, and Au_2Pd_2 Clusters Adsorbed on the T6-Ti-Defect and T6-Si-Defect Sites[a]

T6-Ti-defect			T6-Si-defect		
no.	atom	charge	no.	atom	charge
	Au_5	**−0.35**		**Au_5**	**−0.24**
158	T6 Ti	+1.63	158	T6 Si	+1.87
213	O^s	−0.85	213	O^s	−0.98
214	O^s	−0.82	214	O^s	−0.95
215	O^s	−0.77	215	O^s	−0.97
216	O^s	−0.82	216	O^s	−0.96
	AuPd	**−0.24**		**AuPd**	**−0.22**
	Au	−0.61		Au	−0.61
	Pd	+0.37		Pd	+0.39
158	T6 Ti	+1.53	158	T6 Si	+1.86
213	O^s	−0.84	213	O^s	−0.99
215	O^s	−0.81	215	O^s	−0.98
216	O^s	−0.82	216	O^s	−0.97
	Au_2Pd_2	**−0.25**		**Au_2Pd_2**	**−0.17**
	Au_2	−0.66		Au_2	−0.80
	Pd_2	+0.41		Pd_2	+0.64
158	T6 Ti	+1.53	158	T6 Si	+1.86
213	O^s	−0.83	213	O^s	−0.99
214	O^s	−0.82	214	O^s	−0.95
215	O^s	−0.74	215	O^s	−0.97
216	O^s	−0.74	216	O^s	−0.96

[a] The charge reported for the cluster corresponds to the "net charge" on the whole cluster. The "effective charge" on the Au and Pd portions is also reported for the alloy clusters. For the sake of brevity only important lattice atoms are included.

still negative). Analogous situations are observed for the entire set of clusters reported in this paper.

3.2. Au_3 and Au_4. Unlike for Au_2, we observed an important shape change in the case of adsorbed Au_3. It is well-known that due to Jahn−Teller distortion, the gas-phase Au_3 configuration forms an obtuse-angle triangle (isosceles triangle).[57−59] Upon adsorption, the Au_3 geometry became compact (reduction in the obtuse angle) in all four cases. Compared to the gas-phase Au−Au bond lengths of 2.65, 2.65, and 2.99 Å, bond lengths for adsorbed Au_3 were close to 2.63, 2.75, and 2.82 Å. It should be noted that there are relatively minor differences in the adsorbed geometry of Au_3 on four different types of sites, with ±0.02 Å variation in the aforementioned bond lengths. In all four cases, Au_3 binds in a particular configuration at the intersection of both the channels—one corner Au atom pointing toward the active site and framework around it (QM region), and the other two Au atoms approaching the TS-1 pore center. It is interesting to note that the longest Au−Au bond is between these two Au atoms placed farthest from the T6 site. No particular trend was found regarding the shortest Au−Au bond length. In the case of the nondefect sites, Au_3 BEs are slightly lower than those of Au_2, whereas the reverse is true for the defect sites. A BE of 28.17 kcal/mol for Au_3 anchored on the Ti-defect site is a significant jump from 24.89 kcal/mol for Au_2. Analogous to Au_2, Au_3 adsorption is thermodynamically favorable, as indicated by significantly negative ΔG_{ads}. The closest approach of Au to lattice oxygen is 2.17 Å, again commensurate with the higher binding energy.

There is confusion in the literature about the gas-phase ground-state geometry of neutral Au_4. We found rhombic and Y-shaped geometries to be very close in energy with the Y-shaped geometry about 0.40 kcal/mol lower, a difference lower than the expected error in our DFT calculations. Grönbeck and Andreoni[60] also reported almost degenerate rhombic and Y-shaped geometries. Ding et al.[61] considered Y-shaped Au_4 for their O_2 adsorption studies. However, because the focus of their study was O_2 adsorption, they did not report the difference in the energy of Y-shaped and rhombic Au_4. Landman and coworkers[62] reported a rhombic Au_4 and Mills et al.[63] also chose rhombic Au_4 for their theoretical O_2 adsorption studies. Wang et al.[64] found rhombic Au_4 to be 0.21 eV lower in energy than the Y-shaped Au_4.

Considering the lack of experimental data and aforementioned lack of agreement in the theoretical studies, we considered both rhombic and Y-shaped Au_4 geometries; i.e., both rhombic and Y-shaped geometries were placed in the TS-1 pores and full structural relaxation was allowed to arrive at the adsorbed configuration. We note that the ground states of adsorbed Au_4 with the rhombic starting structure (in the case of all four sites) were ∼0.10 kcal/mol lower in energy than those with Y-shaped starting structure. In calculations with Y-shaped starting point, final adsorbed geometries retained the Y-shape; however, lack of shape change was not always true for rhombic Au_4, as discussed below. We want to point out that in this paper we report our results with a rhombic geometry as the starting configuration. The results obtained with Y-shaped starting structure (not reported) show very similar trends, but with somewhat different absolute numbers.

In the case of rhombic Au_4 adsorbed on nondefect Ti and Si sites, the adsorbed ground-state Au_4 maintained a rhombic shape, but with slight elongation in Au−Au bond lengths. In both cases, the corner Au atom formed the shorter diagonal of the rhombus pointed toward the active site (QM region), and the other Au atom of the shorter diagonal settled near the pore center. The BEs are slightly higher than that observed for Au_3.

Interesting results were found for the defect sites. The rhombic Au_4 placed near the Ti-defect site changed its shape during the geometry optimization and the final configuration was between the rhombic and Y shape (see Figure 6). In this geometry, three Au atoms form a triangle, and the fourth Au atom is collinear with two of the Au atoms of the triangle; these three collinear atoms are situated away from the T6 site with a diagonal orientation in the straight channel. Therefore, the configuration

is not exactly Y-shaped but is an opened-up rhombus approaching the Y shape. No such shape change was found for adsorption on the Si-defect site and the rhombic shape was maintained upon adsorption. Analogous to gas-phase tetramers, all the adsorbed tetramers retained their planar structure. We want to point out that the highest binding energy (30.14 kcal/mol) in this study is for the Au_4 adsorption on the Ti-defect site. Again, adsorption of Au_4 near all four sites is thermodynamically favorable.

Coming to Mulliken charge analysis (similar to Au_2), a charge-polarization was also observed in the case of Au_3 and Au_4. The two (distal) negatively charged Au atoms in Au_3 are located near the pore center, and the cluster was observed to have a net negative charge. These two negatively charged Au atoms exhibit a larger Au−Au distance as a result of intramolecular coulomb repulsion. In all the cases except Au_3 anchored on the Ti-nondefect site, the observed net negative charge on Au_3 was greater than that on Au_2. In the case of both Ti- and Si-nondefect sites, the T6-Ti (or Si) atom and to lesser extent the bridging O atoms of the T6-O−Si linkages lost electron-density to the anchored Au_3. In the case of the defect sites, most of the electron transfer was from T6-Ti (or Si) site. Neighboring O and H atoms of the OH groups contributed to some extent as well. In the case of anchored rhombic Au_4 only the Au atom closest to the active site had a positive charge. However, the Au_4 cluster adsorbed on the Ti-defect site had a Y-shaped configuration, and not only the Au atom closer to the active site but also the Au atom at the center of the three collinear atoms had a slight positive charge, indicating a significant charge-polarization of the adsorbed Au_4 cluster. As discussed for Au_2, the overall mechanism of electron-density transfer from Ti (or Si) sites to adsorbed Au cluster (via lattice O atoms) paralleled by charge-polarization to achieve stability holds true for Au_3 and Au_4 as well.

In all the cases, the net negative charge on Au_4 was close to that found on Au_3. The highest negative charge in the series of five Au clusters was found on the Y-shaped Au_4 adsorbed on Ti-defect site. This observation also explains the change from the original rhombic shape. Both Mills et al.[63] and Ding et al.[61] used a Y-shaped Au_4 anion for their DFT study of O_2 adsorption, which was supported by the theoretical study by Häkkinen and Landman.[62] Most importantly, in their ion-mobility experiments, Furche et al.[65] found that only the Y-shaped anion geometry is consistent with both the experimental data and the vertical detachment energy (VDE) values. The observations of Y-shaped gas-phase Au_4^- and almost −0.43 charge transfer to the Au_4 adsorbed on Ti-defect site, together, explain the shape change from rhombic to the Y-shaped geometry upon adsorption of Au_4. Because in the other three cases less than −0.28 charge is observed on the adsorbed Au_4, we speculate that the effect was not strong enough to result into a major shape change.

3.3. Au_5. We now discuss the case of Au_5 separately, particularly due to the important stearic constraints on Au_5; i.e., the Au_5 cluster barely fits in the 5.5 Å TS-1 pores. The gas-phase structure of Au_5 is a well-established W-shaped planar geometry.[57,60] Upon adsorption, the geometry of Au_5 remained almost the same and both the "W" shape and planarity of Au_5 were retained in all the cases. In the case of nondefect sites, anchored Au_5 was located with most of its portion in the straight channel, and the BE was significantly lower than that for Au_4. In fact, ΔG_{ads} for nondefect sites is close to thermoneutral (slightly positive). Much stronger adsorption at the junction of straight and sinusoidal pores was found for the defect sites, but the BEs were lower than that for Au_4. The orientation of Au_5 anchored on Ti-defect and Si-defect sites was slightly different. In the case of the Ti-defect site, the Au_5 plane was almost situated along the axis of the straight channel, whereas Au_5 was laterally situated in the straight channel on the Si-defect site. In all four cases, one or two Au atoms located at the corner of the two-atom and three-atom sides were pointing toward the T6 site, whereas the rest of the atoms settled near the pore center.

We point out that the net negative charge on the adsorbed Au_5 clusters was much smaller than that observed on Au_{2-4} and the BE followed the trend (smaller for Au_5). The general observation of a positively charged Au atom near the negatively charged lattice O atoms in QM region holds true for Au_5. However, in contrast with Au_{2-4}, there was no definite trend regarding the positive/negative charge on rest of the atoms in adsorbed Au_5. This difference is due to the fact that distal (away from QM region) Au atoms in Au_{2-4} remain near the pore center whereas their analogues in Au_5 are further away from QM region (and pore center) and hence interact with the lattice atoms in the MM region, indicating stearic constraints imposed by TS-1 pores on adsorbed Au_5. Also, in the case of nondefect sites we could not find any one lattice atom/site donating a majority of the electron-density to Au_5; many T sites and lattice O atoms made a small individual contribution. However, in the case of defect sites, T6-Ti (or Si) made a major contribution to the negative charge on the adsorbed Au_5; in the case of Si-defect site, even H atoms of the silanol nest contributed to some extent, mainly due to their high electropositivity.

3.4. AuPd and Au_2Pd_2. We found the gas-phase Au−Pd bond length to be 2.54 Å. Upon adsorption on both Ti- and Si-nondefect sites, a bond length of 2.53 Å was observed, whereas a bond length of 2.57 Å was observed upon adsorption on the defect sites. In all the cases, the adsorbed orientations of the AuPd cluster were very similar; the Pd atom was located closer to the active site and the Au atom was away in the TS-1 pore. Analogous to the cases of Au clusters, stronger adsorption was found on Ti sites than on Si sites, and on defect sites than on nondefect sites. The differences in the binding energies on Ti and Si sites were lower for AuPd than for Au_2.

We investigated a variety of different combinations of atomic placements and several different geometries for Au_2Pd_2 clusters in the gas phase; the details are not reported here but will be reported in the future paper. Because the ground state of the gas-phase Pd_4 cluster is a tetrahedral-like triplet state,[66−68] we investigated both singlet and triplet states for the Au_2Pd_2 cluster. We found a three-dimensional, almost tetrahedral Au_2Pd_2 cluster in the singlet state as the ground-state structure. In Au_2Pd_2, the Au−Pd bond length is 2.69 Å, the Pd−Pd bond length is 2.78 Å, and the Au−Au bond length is 2.90 Å. It is interesting to note that, upon adsorption, the three-dimensional, almost tetrahedral shape of Au_2Pd_2 cluster was retained in all four cases. In all the cases, one of the Pd atoms was pointing toward the active site, and remaining atoms were located in the pores. In general, the BEs for Au_2Pd_2 are smaller than that for Au_4. However, the trends with respect to Ti and Si sites and nondefect and defect sites are also true for Au_2Pd_2.

Because Au clusters extract electron density from the TS-1 lattice and undergo charge polarization, we also studied the effect of alloying with Pd on these processes. In general, Pd atoms preferred to face the negatively charged O atoms in the QM region, whereas the Au atoms preferred to settle near the pore center. In all the cases we found that all the Pd atoms were positively charged, whereas all the Au atoms were negatively charged, and the alloy cluster exhibited a net negative charge. This is not surprising because Au is known to have a much higher electron affinity, ionization potential, and elec-

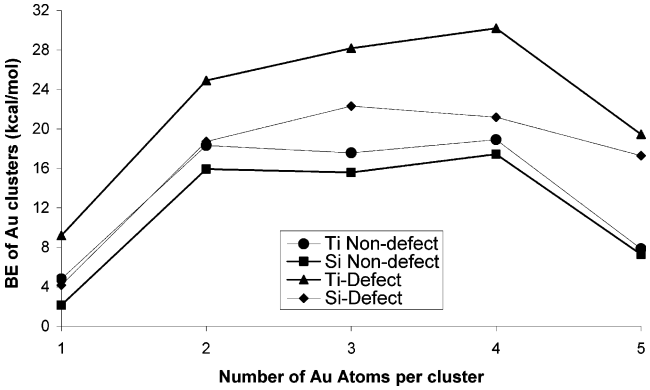

Figure 10. BE versus cluster size (n) for Au_n clusters adsorbed on T6 nondefect and defect sites in TS-1 and S-1.

tronegativity compared to the other noble metals, especially due to strong relativistic effects in Au.[50] The framework atoms that lost electron density to the alloy clusters are same as that found in the case of the pure Au clusters. Again, Coulomb attraction−repulsion with lattice O atoms explains the orientation of AuPd and Au_2Pd_2 clusters. It is interesting to note that alloying with Pd reduced the ability of the clusters to extract electron density from the TS-1 lattice; i.e., the net negative charge on the alloy clusters was smaller (less negative) than that on the equal-sized pure Au clusters probably due to reduced electron affinity upon alloying with Pd.

In summary, the mechanism of electron-density transfer (via lattice O atoms) from Ti (or Si) sites in TS-1 lattice to adsorbed Au clusters paralleled by charge-polarization of the clusters to create favorable interaction with negatively charged lattice O atoms also holds true for AuPd and Au_2Pd_2 clusters.

4. Discussion

4.1. Interpretation of Results. In Figure 10, we show the variation of BE with the Au cluster size for all four types of sites. There exist some general trends: (1) adsorption is stronger on defect sites than on nondefect sites and (2) adsorption is stronger on T6-Ti sites than on T6-Si sites. It is interesting to note that these trends are also obeyed by AuPd and Au_2Pd_2 alloy clusters. The difference in the BEs on Ti and Si sites is more pronounced for defect sites. The higher BEs on the defect sites could be attributed to two factors: (1) more flexibility for the structural relaxation at the defect site and (2) additional electron transfer to Au clusters from the H atoms of the T-OH groups. A third trend is the maximum in the binding energies of Au_n clusters around $n = 3-4$. In some cases, the actual values indicate that adsorption of Au_4 is stronger than that of Au_3.

The arguments made in the previous subsections also explain a relatively lower binding energy for Au_1 than for all other clusters; a negatively charged single Au atom experiences repulsion from the negatively charged lattice O atoms and has no neighboring Au atoms to share its negative-charge burden. The larger clusters orient themselves in such a way that the negatively charged Au atoms settle near the center of the TS-1 pores away from the lattice oxygens. The same explanation may be used to explain the maximum in the electron transfer at around Au_{3-4}. For larger clusters such as Au_5, it is difficult to avoid the repulsion between the negatively charged Au atoms and the lattice O atoms due to stearic constraints imposed by the pore walls. Adsorbed Au_5 clusters have very little flexibility to adjust their orientation to enhance their interaction with the lattice.

Consistent with the net attractive interactions (or net additional stabilization) inside the TS-1 pores, the BE_{MM} values are positive for all seven clusters (Table 1). We also highlight the size-dependence of contributions of force fields to binding energies. The BE_{MM} increases with cluster size for Au_{1-4}, suggesting that the observed BE peak at around $n = 3-4$ is also due to significant contributions from the long-range attractive interactions for Au_3 and Au_4. The BE_{MM} is much smaller for Au_5 than for Au_4 indicating increased contribution of repulsive forces due to shorter distances between atoms in Au_5 and the TS-1 pore wall. The BE_{MM} values for AuPd and Au_2Pd_2 are smaller than for Au_2 and Au_4, respectively, probably due to the difference in the size of the Pd (smaller) and Au atom and due to different force field parameters for Pd and Au. These findings demonstrate the importance of QM/MM calculations in properly modeling adsorption/reaction processes inside the TS-1 pores.

In a recent experimental study from our group, Taylor et al.[16] reported that there is a positive correlation between the Au-loading and the Ti-loading on the high Si/Ti ratio Au/TS-1 catalysts. These results are consistent with our QM/MM calculations, which predict that the Au clusters indeed experience stronger binding on the Ti sites than on the Si sites. Hence, our calculations successfully capture this experimentally observed trend. In addition, a stronger binding of the clusters on Ti sites than on Si sites also indicates that Au clusters adsorbed near the Ti sites may be less susceptible to sintering. In fact, Goodman and co-workers[69] have recently synthesized a titania−silica mixed oxide surface by substitution of Si atoms in SiO_2 by Ti atoms. Through STM experiments they have established that these Ti atoms serve as nucleating sites for Au clusters and lead to sinter-resistant Au/SiO_2-TiO_2 material.[69] However, the Au clusters in their experiments were approximately in the 1−10 nm size range and not as small as in our computational study, and hence a direct comparison between their experiments and our simulations should be carried out with care.

Wells et al.[19] have reported a mechanism in which H_2O_2 attacks the Ti−OH of the T6-Ti-defect site to form Ti−OOH (and H_2O), which subsequently oxidizes propylene to propylene oxide. A possible source of H_2O_2 could be formation on Au clusters from H_2 and O_2, as shown previously by Wells et al.[20] and the current authors[26] for the gas-phase clusters. A possibility of H_2O_2 formation on Au clusters inside the TS-1 lattice cannot be ruled out. Because the strongest binding for all the Au clusters is on the Ti-defect site, H_2O_2 formed (in situ from H_2 and O_2) on Au clusters can readily spill over to Ti-defect sites, forming Ti−OOH. However, an important question is whether there is enough room for H_2O_2 and propylene to attack the active Ti site, which may be covered by the adsorbed Au clusters. On the basis of the geometries we have predicted, it is clear that there is ample space for H_2O_2 and propylene attack on Ti site with Au_{1-2} adsorbed on it as we have found by simply placing peroxide and propylene around the sites. Although Au_5 is quite bulky there is still enough space for peroxide. The question remains, however, whether there is enough room for propylene to adsorb near the Ti site with Au_{3-5} around it. The strongest binding is for Au_3 and Au_4 on the Ti-defect site. Due to the Y-shape of adsorbed Au_4, again, propylene may experience stearic hindrance. Most interesting is the case of adsorbed Au_3; it has the second-highest BE in the whole series and it does not cover the defect site completely. Therefore, it appears that there is enough room for both H_2O_2 and propylene to attack the Ti-defect site. We also point out that upon adsorption of Au_3 and Au_4, Ti−O bond lengths (of the Ti−OH) increased from 1.82 Å (no cluster adsorbed) to 1.91 Å. We speculate that such activation of the Ti−O bond may favor the H_2O_2 attack to form Ti−OOH. However, this speculation can only be verified by

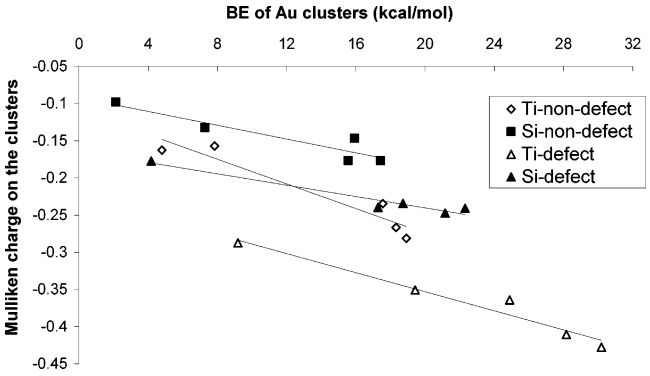

Figure 11. Total Mulliken charge on the adsorbed Au clusters as a function of cluster binding energy for Au_{1-5}. For each type of site, separate linear fits are shown.

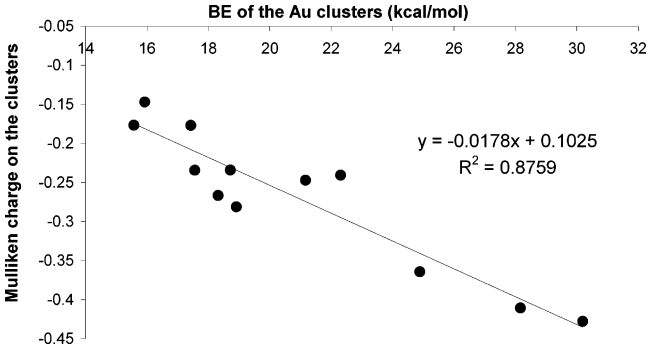

Figure 12. Total Mulliken charge on the adsorbed Au clusters as a function of cluster binding energy for Au_{2-4}. A universal linear fit is shown in the figure.

actually calculating the activation energy for attack of H_2O_2 on Ti site (with Au_3 adsorbed), which is the subject of ongoing investigation.

A comparison of AuPd with Au_2, and Au_2Pd_2 with Au_4, demonstrates that in all the cases the net electron transfer to the alloy clusters is smaller than that to the Au clusters with the same total number of atoms. However, the degree of charge polarization is much higher for alloy clusters than for pure Au clusters, exhibited by greater observed charge separation. This additional electron density on Au may actually enhance the activity of Au clusters as reported recently for CO oxidation using the Na-doped Au_{20} in the DFT study by Molina and Hammer.[70]

The Mulliken charge analysis indicates that the electron-density transfer to Au and Au−Pd clusters is higher in the case of defect sites than for nondefect sites, and higher in the case of T6-Ti-sites than for T6-Si-sites. Because a similar trend was observed for BEs, we now explore a possible correlation between the BE and the charge transfer to the adsorbed clusters.

4.2. Correlation between the Cluster BE and the Charge Transfer to the Cluster. In Figure 11, we plot the net negative Mulliken charge on the adsorbed Au clusters versus the BE of the Au clusters. It is clear that an increase in the electron transfer to the adsorbed Au clusters is associated with higher BEs. Although the trend is not very precise, we point out that the data consists of Au clusters adsorbed on four different types of sites and hence represent four different chemical environments. We also point out that the linear trend is substantially better if one ignores the data points for Au_1 and Au_5; i.e., a rather universal correlation (see Figure 12) exists between the BE and charge transfer for Au_{2-4} adsorbed in four different chemical environments. A better linear trend is obtained by considering the data points for five Au clusters adsorbed on a particular

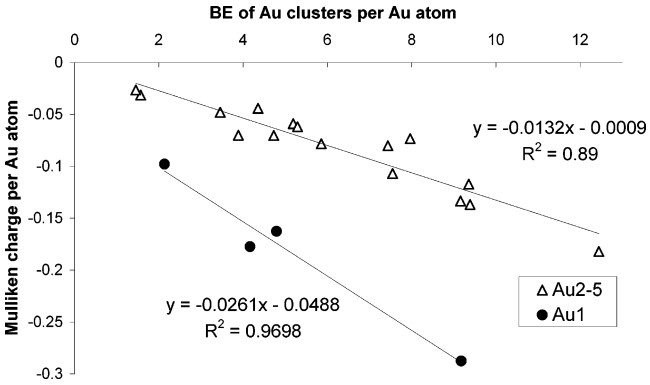

Figure 13. Mulliken charge on the adsorbed Au clusters per Au atom versus cluster binding energy per Au atom for Au_{1-5}. The data in the graph represent four different chemical environments.

site; clearly, in all four cases, the linear trends are excellent (see Figure 11). It is also clear from the Figure 11 that there is a higher charge transfer to Au clusters anchored on the Ti sites compared to Si sites, which results in large BEs on the Ti sites. A stronger binding on defect sites is also consistent with the higher charge transfer, particularly due to the H atoms of the T−OH groups, which donates electron density to Au clusters.

In Figure 13, we show a correlation between BE per Au atom and charge transfer per Au atom. The points for Au_1 follow a separate line, whereas points for all other clusters lie on the same line. The difference is due to the positive charge on the Au atoms of Au_{2-5} facing the QM region, which reduces the overall negative charge per atom for these clusters, whereas Au_1 always has a negative charge on it. Therefore, there is excess negative charge per Au atom in the case of Au_1. The universal linear correlation for Au_{2-5} (in four different chemical environments) is quite good and we point out that the line passes through the origin, indicating that the BE per Au atom is zero when electron transfer per Au atom is zero.

As stated earlier, Au clusters have high electron affinity, and we tried to correlate cluster electron affinities with binding energies but could not find a direct correlation. This is because cluster BEs have the following closely related contributions: (1) electron-affinity contribution via the net negative charge on the adsorbed clusters, (2) attraction/repulsion with the lattice oxygens, (3) geometry relaxation effects, and (4) the long-range interactions due to dispersion forces. Because the negatively charged Au atoms tend to locate away from the active QM region, Coulomb attraction between the lattice O atoms and the (positively charged) Au atom(s) closest to them contributes to the BE. Crudely speaking, Coulomb repulsion reduces the binding energy of Au_5, whereas Au_{2-4} manage to reduce this repulsion due to lesser stearic constraints and have BEs near the peak. In addition, exact values of electron affinities really refer to clusters with full −1 charge on them, which is certainly not the case for adsorbed Au clusters.

4.3. Thermochemistry. So far we have discussed only the electronic energies of adsorption (ΔE_{ads}) at 0 K in a vacuum. Again, we note that BE $= -\Delta E_{ads}$; i.e., a positive binding energy means negative ΔE_{ads} (exothermic). However, ΔE_{ads} is not a thermodynamic quantity and hence we carried out a full thermochemical analysis at 298.15 K and 1 atm (Table 7). It is clear that due to loss in entropy upon adsorption, ΔG_{ads} is less negative than ΔE_{ads}. In fact, in some cases the ΔG_{ads} is positive, indicating a thermodynamically unfavorable adsorption at 298.15 K. This highlights the importance of doing thermochemical analysis and using ΔG_{ads} to interpret the adsorption energetics. However, we point out that all the thermodynamically important

TABLE 7: Thermochemical Analysis of Adsorption of Au_{1-5} Clusters Inside the TS-1 Pores at 298.15 K and 1 atm[a]

Au cluster size (n)	$\Delta E_{ZPE,ads}$ (kcal/mole)		ΔU_{ads} (kcal/mole)		ΔG_{ads} (kcal/mole)	
	Ti site	Si site	Ti site	Si site	Ti site	Si site
Nondefect Sites						
1	−5.04	−2.27	−4.24	−1.44	+1.79	+4.01
2	−18.11	−15.83	−17.06	−14.78	−8.19	−6.23
3	−17.59	−15.60	−16.64	−14.06	−3.54	−4.57
4	−18.84	−17.44	−17.36	−16.02	−8.13	−5.17
5	−7.92	−7.34	−6.26	−5.69	+3.85	+4.33
Defect Sites						
1	−8.71	−4.25	−8.00	−3.41	−1.38	+2.64
2	−23.96	−18.11	−22.95	−17.01	−13.91	−8.25
3	−27.12	−21.62	−25.70	−20.07	−14.95	−9.55
4	−29.30	−20.61	−27.96	−19.08	−17.29	−8.97
5	−18.21	−16.83	−16.64	−15.25	−5.83	−4.09

[a] $\Delta E_{ZPE,ads}$ is the zero-point energy corrected adsorption energy, ΔU_{ads} is the internal energy of adsorption at 298.15 K and 1 atm, and ΔG_{ads} is the Gibbs free energy of adsorption at 298.15 K and 1 atm.

energies including ΔG_{ads} show exactly the same trends as shown by BE ($-\Delta E_{ads}$). Clearly, adsorption is more favorable on Ti sites than on Si sites, and on defect sites than on nondefect sites. Also, ΔG_{ads} is most favorable around $n = 3-4$ (Table 7).

The results reported in this paper are also useful to predict the sintering behavior of adsorbed Au clusters; weakly adsorbed clusters will be mobile on the walls of TS-1 pores and hence will have greater probability of sintering due to agglomeration with each other or with other strongly adsorbed clusters. Again, we note the importance of using ΔG_{ads} to arrive at our conclusions. On the basis of our results, we cannot study the kinetics of cluster diffusion or sintering but can only identify the clusters that may undergo sintering (based on ΔG_{ads}). It is clear from Table 7 that Au_1 and Au_5 clusters adsorbed on Ti/Si-nondefect sites have positive ΔG_{ads} and may have a tendency to diffuse along the pore walls. Of course, due to the difference between size and mass of Au_1 and Au_5, mobility of Au_5 clusters could be much smaller than that of Au_1 clusters. In all the cases Au_2, Au_3, and Au_4 have significantly negative ΔG_{ads} and may have negligible mobility. Interestingly, in their elegant experiments on deposition of small size-selected intact Au clusters on TiO_2-(110), Tong et al.[71] found that Au_1 clusters are highly mobile and hence sinter to larger sizes, whereas larger clusters (Au_{2-8}) have much less mobility and do not undergo sintering. In general, a more favorable adsorption on the defect sites implies that presence of defects in the TS-1 framework may reduce mobility and hence sintering of the Au clusters. This finding has important implications in synthesis of TS-1 and Au/TS-1 catalyst.

5. Conclusions

We used hybrid QM/MM calculations to study the interaction of small Au and Au−Pd alloy clusters with the interior of the TS-1 lattice. We modeled four different kinds of environments by considering four different types of sites: (1) T6-Ti-nondefect, (2) T6-Si-nondefect, (3) T6-Ti-defect, and (4) T6-Si-defect. The T6 site, which lies at the intersection of the straight and sinusoidal channels, is also a candidate for the Ti substitution.[25] In most of the cases, the clusters preferred to bind at the intersection of the straight and the sinusoidal pores and (Au clusters) retained their planarity upon adsorption.

Our calculations captured following general trends: (1) a stronger binding on Ti-sites than on Si-sites, (2) a stronger binding on defect sites than on nondefect sites, and (3) a maximum in the BE of the Au_n clusters at around $n = 3-4$. These trends were also verified by rigorous thermochemical calculations (ΔG_{ads}). The trend (1) is consistent with the experimental observation of a positive correlation between the Ti-loading and the Au-loading on the Au/TS-1 catalysts.[16] In light of the previously reported hydrogen peroxide formation pathway from H_2 and O_2 (on Au clusters)[20,26] and propylene oxidation through attack of H_2O_2 at Ti-defect site,[19] it is interesting to note that stronger binding of Au clusters on defect sites points at a potential spill-over of H_2O_2 formed on Au clusters to adjacent Ti-defect site. This is important in the context of a potential direct propylene epoxidation mechanism using H_2 and O_2 over Au/TS-1 catalysts, which could be feasible inside the pores of TS-1. In this context, a case of Au_3/Ti-defect is of primary importance due to the space available for the attack of H_2O_2 and propylene on active Ti site. We note that upon Au_3 adsorption, the Ti−OH bond length increased from 1.82 to 1.91 Å, which is an indication of the potential activation of the Ti−O bond. We also note that some of the adsorbed Au clusters do not block the Ti sites completely, indicating that site poisoning is not likely a serious issue.

In all the cases, there is a net negative charge on the adsorbed clusters ranging from −0.1 to −0.45. In fact, the charge transfer was highest for the Au_4 adsorbed on the Ti-defect site and resulted into a shape change of Au_4 from rhombic in the gas phase to Y-shaped in the adsorbed state—consistent with the experimental finding of Y-shaped Au_4^- cluster in the gas phase.[65] In the case of the clusters with more than one atom, the Au/Pd atom(s) facing the active site (QM region) were positively charged, whereas negatively charged Au atoms settled near the center of the pores to minimize the Coulomb repulsion with the negatively charged lattice oxygens. The Coulomb interactions along with stearic constraints in the TS-1 pores explain a relatively lower BE of Au_5, whereas lack of neighboring Au atoms to share negative charge explains the lowest BE of Au_1. Therefore, charge analysis is useful in explaining a maximum in the BE versus Au-cluster size.

In general, electron transfer to adsorbed clusters was larger on Ti sites than at Si sites, and larger on defect sites than on nondefect sites. Considering the high electron-affinity of the Au clusters, it is not surprising that the electron transfer from the TS-1 to the adsorbed clusters results into a positive BE. However, there are additional contributions to the BE due to the Coulomb attraction−repulsion between the charged Au atoms and the negatively charged lattice O atoms, geometry relaxation, and the dispersion interactions. In the case of Au−Pd clusters, net electron transfer to the adsorbed clusters was lower than that in the case of pure Au clusters of the same size; this is due to a much lower electron-affinity of Pd than of Au. Also, Pd atoms, which always faced the TS-1 lattice, were positively charged and Au atoms, located near the pore center, were negatively charged.

We also found a correlation between the extent of electron transfer or net negative charge on the Au clusters and the cluster BE—the higher the negative charge on the Au clusters, the higher the observed BE. Comparing BE per atom versus negative charge per atom of the adsorbed clusters also shows a linear correlation, which is universal for Au_{2-5} adsorbed on four different kinds of sites. We point out that these correlations pass through origin; i.e., BE (per atom) is zero when there is no electron transfer. This means that electronic factors are important in Au−support (TS-1) interactions and in certain cases may induce significant geometry changes, e.g., Au_4 adsorbed on the Ti-defect site. Our calculations suggest that Au_1 and to some

extent Au_5 clusters may undergo sintering due to their high mobility (weak adsorption). Finally, the presence of defects in TS-1 may reduce the sintering of the adsorbed Au clusters in Au/TS-1 catalyst.

Acknowledgment. This work was funded by the National Science Foundation through the grant CTS-0238989-CAREER (K.T.T.) and by the United States Department of Energy, Office of Basic Energy Sciences, through the grant DE-FG02-01ER-15107 (W.N.D.). Computational resources were obtained through a grant from the National Computational Science Alliance (AAB proposal ESC030001) and through the supercomputing resources at Purdue University. A.M.J. thanks Yogesh Joshi, Dr. David Wells, Dr. Aditya Bhan, Dr. Bradley Taylor, and Lasitha Cumaranatunge for their assistance and valuable suggestions.

Supporting Information Available: The effect of using a more complete basis set augmented with diffuse and polarization functions on the binding energy of Au_3 and charge transfer to Au_3 adsorbed on four different types of sites was investigated. This material is available free of charge via the Internet at http://pubs.acs.org.

References and Notes

(1) Hammer, B.; Nørskov, J. K. *Nature* **1995**, *376*, 238.
(2) Haruta, M.; Yamada, N.; Kobayashi, T.; Iijima, S. *J. Catal.* **1989**, *115*, 301.
(3) Haruta, M.; Tsubota, S.; Kobayashi, T.; Kangeyama, H.; Genet, M. J.; Delmon, B. *J. Catal.* **1993**, *144*, 175.
(4) Haruta, M. *Catal. Today* **1997**, *36*, 153.
(5) Haruta, M.; Date, M. *Appl. Catal. A* **2001**, *222*, 427.
(6) Guzman, J.; Gates, B. C. *J. Phys. Chem. B* **2002**, *106*, 7659.
(7) Guzman, J.; Gates, B. C. *J. Phys. Chem. B* **2003**, *107*, 2242.
(8) Guzman, J.; Gates, B. C. *J. Am. Chem. Soc.* **2004**, *126*, 2672.
(9) Guzman, J.; Carrettin, S.; Fierro-Gonzalez, J. C.; Hao, Y.; Gates, B. C.; Corma, A. *Angew. Chem., Int. Ed.* **2005**, *44*, 4778.
(10) Stangland, E. E.; Stavens, K. B.; Andres, R. P.; Delgass, W. N. *J. Catal.* **2000**, *191*, 332.
(11) Stangland, E. E.; Taylor, B.; Andres, R. P.; Delgass, W. N. *J. Phys. Chem. B* **2005**, *109*, 2321.
(12) Uphade, B. S.; Yamada, Y.; Akita, T.; Nakamura, T.; Haruta, M. *Appl. Catal. A* **2001**, *215*, 137.
(13) Uphade, B. S.; Akita, T.; Nakamura, T.; Haruta, M. *J. Catal.* **2002**, *209*, 331.
(14) Nijhuis, T. A.; Huizinga, B. J.; Makkee, M.; Moulijn, J. A. *Ind. Eng. Chem. Res.* **1999**, *38*, 884.
(15) Nijhuis, T. A.; Visser, T.; Weckhuysen, B. M. *Angew. Chem., Int. Ed.* **2005**, *44*, 1115.
(16) Taylor, B.; Lauterbach, J.; Delgass, W. N. *Appl. Catal. A* **2005**, *291*, 188.
(17) Cumarantunge, L.; Delgass, W. N. *J. Catal.* **2005**, *232*, 38.
(18) Yap, N.; Andres, R. P.; Delgass, W. N. *J. Catal.* **2004**, *226*, 156.
(19) Wells, D. H.; Delgass, W. N.; Thomson, K. T. *J. Am. Chem. Soc.* **2004**, *126*, 2956.
(20) Wells, D. H.; Delgass, W. N.; Thomson, K. T. *J. Catal.* **2004**, *225*, 69.
(21) Mavrikakis, M.; Stoltze, P.; Nørskov, J. K. *Catal. Lett.* **2000**, *64*, 101.
(22) Lopez, N.; Nørskov, J. K. *Surf. Sci.* **2002**, *515*, 175.
(23) Sanchez, A.; Abbet, S.; Heiz, U.; Schneider, W.-D.; Häkkinen, H.; Barnett, R. N.; Landman, U. *J. Phys. Chem. A* **1999**, *103*, 9573.
(24) Landon, P.; Collier, P. J.; Carley, A. F.; Chadwick, D.; Papworth, A. J.; Burrows, A.; Kiely, C. J.; Hutchings, G. J. *Phys. Chem. Chem. Phys.* **2003**, *5*, 1917.
(25) Lamberti, C.; Bordiga, S.; Zecchina, A.; Artioli, G.; Marra, G.; Spanò, G. *J. Am. Chem. Soc.* **2001**, *123*, 2204.
(26) Joshi, A. M.; Delgass, W. N.; Thomson, K. T. *J. Phys. Chem. B* **2005**, *109*, 22392.
(27) Joshi, A. M.; Delgass, W. N.; Thomson, K. T. *J. Phys. Chem. B* **2006**, *110*, 2572.
(28) Sauer, J.; Sierka, M. *J. Comput. Chem.* **2000**, *21*, 1470.
(29) Sierka, M.; Sauer, J. *Faraday Discuss.* **1997**, *106*, 41.
(30) Kasuriya, S.; Namuangruk, S.; Treesukol, P.; Tirtowidjojo, M.; Limtrakul, J. *J. Catal.* **2003**, *219*, 320.
(31) Namuangruk, S.; Pantu, P.; Limtrakul, J. *J. Catal.* **2004**, *225*, 523.
(32) Solans-Monfort, X.; Sodupe, M.; Branchadell, V.; Sauer, J.; Orlando, R.; Ugliengo, P. *J. Phys. Chem. B* **2005**, *109*, 3539.
(33) Nieminen, V.; Sierka, M.; Murzin, D. Y.; Sauer, J. *J. Catal.* **2005**, *231*, 393.
(34) Hill, J.-R.; Sauer, J. *J. Phys. Chem.* **1994**, *98*, 1238.
(35) Rappe, A. K.; Casewit, C. J.; Colwell, K. S.; Goddard, W. A.; Skiff, W. M. *J. Am. Chem. Soc.* **1992**, *114*, 10024.
(36) Solans-Monfort, X.; Bertran, J.; Branchadell, V.; Sodupe, M. *J. Phys. Chem. B* **2002**, *106*, 10220.
(37) Joshi, Y. V.; Thomson, K. T. *J. Catal.* **2005**, *230*, 440.
(38) Joshi, Y. V.; Thomson, K. T. *Catal. Today* **2005**, *105*, 106.
(39) Jiang, N.; Yuan, S.; Wang, J.; Qin, Z.; Jiao, H.; Li, Y.-w. *J. Mol. Catal. A* **2005**, *232*, 59.
(40) Dapprich, S.; Komaromi, I.; Byun, K. S.; Morokuma, K.; Frisch, M. J. *J. Mol. Struct. THEOCHEM* **1999**, *461*, 1.
(41) Frisch, M. J.; Trucks, G. W.; Schlegel, H. B.; Scuseria, G. E.; Robb, M. A.; Cheeseman, J. R.; Montgomery, J. A., Jr.; Vreven, T.; Kudin, K. N.; Burant, J. C.; Millam, J. M.; Iyengar, S. S.; Tomasi, J.; Barone, V.; Mennucci, B.; Cossi, M.; Scalmani, G.; Rega, N.; Petersson, G. A.; Nakatsuji, H.; Hada, M.; Ehara, M.; Toyota, K.; Fukuda, R.; Hasegawa, J.; Ishida, M.; Nakajima, T.; Honda, Y.; Kitao, O.; Nakai, H.; Klene, M.; Li, X.; Knox, J. E.; Hratchian, H. P.; Cross, J. B.; Bakken, V.; Adamo, C.; Jaramillo, J.; Gomperts, R.; Stratmann, R. E.; Yazyev, O.; Austin, A. J.; Cammi, R.; Pomelli, C.; Ochterski, J. W.; Ayala, P. Y.; Morokuma, K.; Voth, G. A.; Salvador, P.; Dannenberg, J. J.; Zakrzewski, V. G.; Dapprich, S.; Daniels, A. D.; Strain, M. C.; Farkas, O.; Malick, D. K.; Rabuck, A. D.; Raghavachari, K.; Foresman, J. B.; Ortiz, J. V.; Cui, Q.; Baboul, A. G.; Clifford, S.; Cioslowski, J.; Stefanov, B. B.; Liu, G.; Liashenko, A.; Piskorz, P.; Komaromi, I.; Martin, R. L.; Fox, D. J.; Keith, T.; Al-Laham, M. A.; Peng, C. Y.; Nanayakkara, A.; Challacombe, M.; Gill, P. M. W.; Johnson, B.; Chen, W.; Wong, M. W.; Gonzalez, C.; Pople, J. A. *Gaussian 03*, revision C.02; Gaussian, Inc.: Wallingford, CT, 2004.
(42) Atoguchi, T.; Yao, S. *J. Mol. Catal. A* **2003**, *191*, 281.
(43) Ricchiardi, G.; de Man, A.; Sauer, J. *Phys. Chem. Chem. Phys.* **2000**, *2*, 2195.
(44) Perdew, J. P.; Burke, K.; Wang, Y. *Phys. Rev. B* **1996**, *54*, 16533.
(45) Perdew, J. P.; Chevary, J. A.; Vosko, S. H.; Jackson, K. A.; Pederson, M. R.; Singh, D. J.; Fiolhais, C. *Phys. Rev. B* **1992**, *46*, 6671.
(46) Perdew, J. P.; Chevary, J. A.; Vosko, S. H.; Jackson, K. A.; Pederson, M. R.; Singh, D. J.; Fiolhais, C. *Phys. Rev. B* **1993**, *48*, 4978.
(47) Hay, P. J.; Wadt, W. R. *J. Chem. Phys.* **1985**, *82*, 270.
(48) Hay, P. J.; Wadt, W. R. *J. Chem. Phys.* **1985**, *82*, 299.
(49) Henry, P. F.; Weller, M. T.; Wilson, C. C. *J. Phys. Chem. B* **2001**, *105*, 7452.
(50) Pyykkö, P. *Angew. Chem., Int. Ed.* **2004**, *43*, 4412.
(51) Del Vitto, A.; Pacchioni, G.; Lim, K. H.; Rösch, N.; Antonietti, J. M.; Michalski, M.; Heiz, U.; Jones, H. *J. Phys. Chem. B* **2005**, *109*, 19876.
(52) Antonietti, J. M.; Michalski, M.; Heiz, U.; Jones, H.; Lim, K. H.; Rösch, N.; Del Vitto, A.; Pacchioni, G. *Phys. Rev. Lett.* **2005**, *94*, 213402.
(53) Giordano, L.; Del Vitto, A.; Pacchioni, G. *J. Chem. Phys.* **2006**, *124*, 034701.
(54) Vijay, A.; Mills, G.; Metiu, H. *J. Chem. Phys.* **2003**, *118*, 6536.
(55) Taylor, K. J.; Pettiette-Hall, C. L.; Cheshnovsky, O.; Smalley, R. E. *J. Chem. Phys.* **1992**, *96*, 3319.
(56) Hotop, H.; Lineberger, W. C. *J. Phys. Chem. Ref. Data* **1975**, *4*, 539.
(57) Bravo-Pèrez, G.; Garzòn, I. L.; Novaro, O. *J. Mol. Struct. THEOCHEM* **1999**, *493*, 225.
(58) Wesendrup, R.; Hunt, T.; Schwerdtfeger, P. *J. Chem. Phys.* **2000**, *112*, 9356.
(59) Howard, J. A.; Sutcliffe, R.; Mile, B. *Surf. Sci.* **1985**, *156*, 214.
(60) Grönbeck, H.; Andreoni, W. *Chem. Phys.* **2000**, *262*, 1.
(61) Ding, X.; Li, Z.; Yang, J.; Hou, J. G.; Zhu, Q. *J. Chem. Phys.* **2004**, *120*, 9594.
(62) Häkkinen, H.; Landman, U. *Phys. Rev. B* **2000**, *62*, R2287.
(63) Mills, G.; Gordon, M. S.; Metiu, H. *Chem. Phys. Lett.* **2002**, *359*, 493.
(64) Wang, J.; Wang, G.; Zhao, J. *Phys. Rev. B* **2002**, *66*, 035418.
(65) Furche, F.; Ahlrichs, R.; Weis, P.; Jacob, C.; Gilb, S.; Bierweiler, T.; Kappes, M. M. *J. Chem. Phys.* **2002**, *117*, 6982.
(66) Nava, P.; Sierka, M.; Ahlrichs, R. *Phys. Chem. Chem. Phys.* **2003**, *5*, 3372.
(67) Dai, D.; Balasubramanian, K. *J. Chem. Phys.* **1995**, *103*, 648.
(68) Zacarias, A. G.; Castro, M.; Tour, J. M.; Seminario, J. M. *J. Phys. Chem. A* **1999**, *103*, 7692.
(69) Min, B. K.; Wallace, W. T.; Goodman, D. W. *J. Phys. Chem. B* **2004**, *108*, 14609.
(70) Molina, L. M.; Hammer, B. *J. Catal.* **2005**, *233*, 399.
(71) Tong, X.; Benz, L.; Kemper, P.; Metiu, H.; Bowers, M. T.; Buratto, S. K. *J. Am. Chem. Soc.* **2005**, *127*, 13516.